FULL PAPER

Reconfigurable Anisotropic Coatings via Magnetic Field-Directed Assembly and Translocation of Locking Magnetic Chains

Alexander Tokarev, Yu Gu, Andrey Zakharchenko, Oleksandr Trotsenko, Igor Luzinov, Konstantin G. Kornev, and Sergiy Minko**

A method for the generation of remotely reconfigurable anisotropic coatings is developed. To form these coatings, locking magnetic nanoparticles (LMNPs) made of a superparamagnetic core and a two-component polymer shell are employed. Two different polymers form phase-separated coaxial shells. The outer shell provides repulsive interactions between the LMNPs while the inner shell exerts attractive forces between the particles. Applying a non-uniform magnetic field, one gathers the particles together, pushing them to come in contact when the internal shells could effectively hold the particles together. When the magnetic field is turned off, the particles remain locked due to these strong interactions between internal shells. The shells are thus made stimuli-responsive, so this locking can be made reversible and the chains can be disintegrated on demand. In a non-uniform magnetic field, the assembled chains translocate, bind to the solid substrate and form anisotropic coatings with a "locked" anisotropic structure. The coatings can be constructed, aligned, realigned, degraded, and generated again on demand by changing the magnetic field and particle environment. The mechanism of the coating formation is explained using experimental observations and a theoretical model.

1. Introduction

Magnetic-field-directed assembly of the superparamagnetic nanoparticles provides a number of intriguing opportunities for the nanotechnology and material science including the remote control of the particle self-assembly and the generated structures and generation of anisotropic nanostructured materials.[1] The ability of magnetic fluids to form chains of magnetic particles in a magnetic field[2] is being used to form anisotropic composites when alignment of the magnetic nanoparticles in a monomer solution or a polymer melt is followed by polymerization, crosslinking, glass or crystallization transitions.[1c,3]

Optical, mechanical, electrical, and thermal properties of nanocomposites can be tuned by changing the materials anisotropy with a magnetic field during the composite formation.[4] The magnetic nanocomposites (as any other fiber loaded composites)[3e] are reinforced by magnetic chains.[3b,5] The synthesized nanocomposites show mechanical,[6] thermal,[5b,c] and optical anisotropy[3a,7] and can be used to create patterned microstructures with controllable periodicity,[8] materials with magnetically controlled anisotropic porosity,[9] magnetically controlled MEMS devices for drug delivery,[10] tunable diffraction gratings,[11] magnetic actuators for microfluidics,[12] dynamic absorbers,[13] and electromagnetic shielding composites.[14] Thermal properties[5b,c] and conductivity[15] of materials can be controlled by changing the directions of the applied magnetic field during the composite formation. Fabrication of complex composite materials with combination of different physical properties calls for the development of new tools and methodologies. It is desirable to control the alignment and interactions of the building blocks constituting the composite material; especially important is to control the interactions between the blocks by switching them from attractive to repulsive and vice versa. Making the building blocks magnetic and applying magnetic field, one provides the versatile possibilities to direct the assembly and control the interactions between the blocks.

To date, there have been several successful strategies for formation of stable chains/nanowires from nanoparticles as the building blocks of these 1D structures.[16] These 1D structures can be made through the template-directed synthesis inside the channels in solids or other mesostructures self-assembled from block copolymers, cylindrical polymer brushes, 1D biological

Dr. A. Tokarev, A. Zakharchenko, O. Trotsenko, Prof. S. Minko
Department of Chemistry and Biomolecular Science
Clarkson University
Potsdam, New York 13699, USA
E-mail: sminko@uga.edu
Dr. A. Tokarev, A. Zakharchenko, O. Trotsenko, Prof. S. Minko
Nanostructured Materials Laboratory
the University of Georgia
Athens, Georgia 30602, USA
Y. Gu, Prof. I. Luzinov, Prof. K. G. Kornev
Department of Materials Science and Engineering
Clemson University
Clemson, South Carolina 29634, USA
E-mail: kkornev@clemson.edu

DOI: 10.1002/adfm.201303358

templates, and other existing 1D templates. There is a set of other methods for formation of 1D structures: electrospinning of fibers; magnetic field-directed formation of the chains combined with the chemical cross-linking and stabilization; and kinetically driven nanowire formation by persistency (self-templating).[17] The field-directed particle assembly[18] is a scalable method enabling control of the particle assembly in suspensions via the field-induced polarization and strong dipole–dipole interparticle interactions with the energies exceeding kT.[19] In fact, particles in collidal dispersions are traditionally stabilized electrostatically and sterically using the particle surface charge, surfactants, and/or polymers. Thus, if the particles are not chemically or physically locked together and when the external field is turned off, the structures made in the colloidal dispersion are destroyed by the thermal motion.

Turning the external field on/off one can control the structure and rheology of materials and fluids;[20] or direct the synthesis of the 2D and 3D colloidal crystals by exposing these dispersions to static or oscillatory fields for some time.[21] More complex anisotropic structures can be attained by using non-spherical particles[22] of forming the structures at the interfaces[23] causing the spatial constrain for the particle assembly.

A scalable field-directed formation of stablechains of magnetic nanoparticles has been reported recently. It has been shown that the permanent locking of the structures after removal of the magnetic field can be achieved via covalent bonding. For instance, as shown previously,[24] ferromagnetic cobalt (Co) nanoparticles can be assembled into strings at a cross-linkable oil-water interface. These structures can be formed under the field or without field. The nanoparticles were permanently fixed into the 1D mesoscopic polymer chains (1–9 μm) via photopolymerization. Another example demonstrated that the stable chains of Co nanoparticles can be produced by modifying the chains formed under the magnetic field with a block copolymer.[25] The coating was then cured by photo-cross-linking the copolymer layer. As a result, stable (without magnetic field) nanoparticle wires and solvent-dispersible Co nanoparticle wires were obtained. Furst's group reported a method of making the permanently linked monodisperse paramagnetic chains[26] by covalently linking the surface-functionalized (with NH_2 groups) polystyrene/magnetite particles. The particle linking was achieved by forcing gluteraldehyde to react with the amine groups on the neighboring surfaces.

Non-covalent formation of stable magnetic nanowires by polymer bridging was reported by Goubault et al.[27] The magnetic colloids were first covered with adsorbed polyacrylic acid, which contributes to their colloidal stability by inducing entropic repulsive forces. When magnetic field was applied, the colloids formed chains. The chains were pushed together leading to interpenetration of their adsorbed polymer layers. Under proper conditions, the dynamics of the confined layers led to bridging, making the filament formation irreversible after removal of the magnetic field. Xiong et al.[28] used the polymer bridging approach to obtain Co nanowires stabilized by polyvinylpyrrolidone. Corr et al.[29] employed a polyelectrolyte (polysodium-4-styrene sulfonate) to generate stable (due to the interpenetration of the polymer shells) magnetite particle chains. Documented studies indicate that the filed-directed assembly in combination with the polymer surface modification is an effective tool to obtain stable chains/nanowires made of magnetic particles. However, there is less understanding how the magnetic-field-directed assembly could be applied for formation of the particle coatings at interfaces.

In this work we develop the magnetic-field-directed assembly of anisotropic thin films and coatings that can be changed, erased and reconfigured using the locking magnetic nanoparticles (LMNPs). The concept of LMNPs has been recently introduced in the literature.[30] LMNPs are core-shell magnetic nanoparticle with a superparamagnetic core and a polymeric shell. The polymeric shell is made of two different materials which form two stratified (coaxial) shells when the outer shell induces repulsive forces between LMNPs while the inner shell exerts attractive forces between particles. The density and thickness of each shell are adjusted in such a way that LMNPs form stable colloidal dispersions. Applying a non-uniform magnetic field, one gathers the particles together pushing them to come in contact when the internal shells could effectively hold the particles together. When the magnetic field is turned off the particles remain locked due to these strong interactions between internal shells. These attractive interactions are stronger than the repulsive ones and the generated magnetic chains are not destroyed by thermal fluctuations. The locking is reversible and the chains can be unlocked and disintegrated by using some stimuli in the liquid carrier.

Here we introduce the magnetic-field-directed assembly when the reconfigurable magnetic coatings are formed by a forest of magnetic chains made of LMNPs. LMNPs form chains in the external magnetic field. The chains are directed to the surface of the solid substrate by the non-uniform magnetic field toward the highest field gradient. The array of the chains, that are arriving to the substrate surface, is stabilized when the LMNPs are bound in the chains and the chains are bound to the substrate via locking mechanism. Thus, the anisotropic coatings can be generated, stabilized, aligned and disintegrated on demand by locking and unlocking stimuli.

2. Results in Discussion

2.1. Formation of Coatings

In this work we synthesized 9.5 ± 1 nm Fe_3O_4 nanoparticles encapsulated in a 38 ± 5 nm thick silica shell and decorated with a covalently grafted poly(2-vinylpyridine-*block*-ethylene oxide) (P2VP-*b*-PEO) block copolymer. The synthesis of LNPS was described elsewhere[30] (see experimental details in the Supporting Information, SI). Structure of nanoparticles was analyzed with TEM and is discussed later in the text. Multiple core nanoparticles were synthesized intentionally for these experiments. Multiple magnetic cores in the nanoparticles result in the increased magnetization and, thus, in a decreased time for the composite coating formation. The latter is a critical parameter in the process of the composite formation. Magnetic properties of Fe_3O_4 particles coated with silica were characterized by Alternating Gradient Magnetometer at 25 °C (AGM 2900, Princeton Inc.). As shown in Figure S1 in SI, the particles are superparamagnetic without spontaneous magnetization.

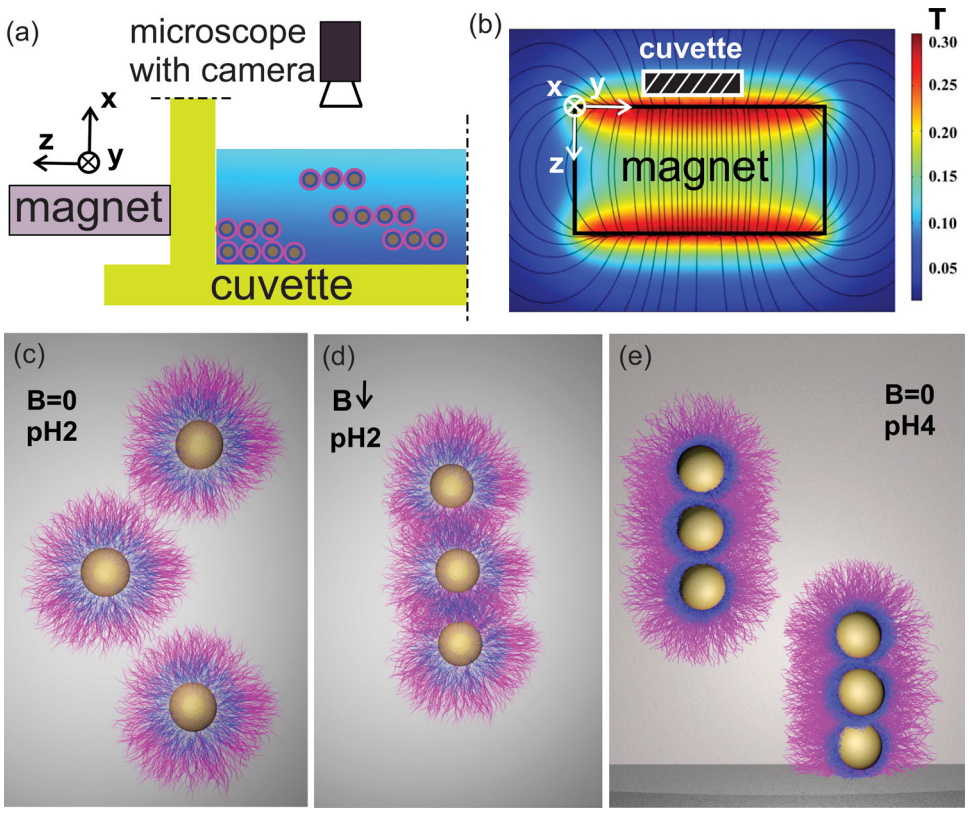

Figure 1. Schematics of the experimental set up and mechanism of locking: a) a fluidic cell is made of two glass sheets arranged to form a T-shape configuration that accommodates a droplet of an LMNP suspension; the magnet is placed behind the glass as shown in the scheme and the cells is placed on the stage of an dark field optical microscope; LMNPs form chains and these chains are moved towards the glass surface by the non-uniform magnetic field generating a forest-like structure on the surface. For simplicity, particles are shown having a single magnetic core in all figures. b) Magnetic field distribution in the cuvette area is calculated numerically with COMSOL (http://www.comsol.com). The observations were taken at the spot centered at z = –2 mm, y = 12.8 mm; c) LMNPs form stable suspension at pH < 4 when both PEO (red) and P2VP (blue) shells contribute to repulsive interaction between LMNPs; d) The particles are aligned in magnetic field directed downward as shown by the arrow to form chains; e) At pH > 4, hydrophobic interaction stabilize chains when attraction between the inner hydrophobic shells is stronger than repulsion between outer shells; the chains are attached to the solid substrate via the inner shell.

Generation of magnetic chains and their translocation was monitored using an experimental setup shown in **Figure 1**a. A 2 µL droplet of the LMNPs dispersion (0.8 g/L) was placed on the surface of a glass slide. A rectangular neodymium magnet (magnetized in z-direction) was positioned at 2 mm distance from the surface of the glass slide (Figure 1a,b). The magnetic field was mapped using a digital teslameter (133-DG GMW Inc.) and COMSOL solver (Figure 1b). Chain formation was recorded with an optical microscope equipped with a video camera.

The nanoparticle locking is triggered by changing pH in the colloidal dispersion (Figure 1c–e). The locking mechanism is turned on at pH > 4 when P2VP chains are hydrophobic and the particle-particle interactions are hydrophobic in aqueous suspension. At pH < 4, P2VP is ionized and positively charged. That results in repulsive interactions between particles due to electrostatic and steric forces. Hence, the chains are stabilized at pH > 4 and disintegrated at pH < 4.

No visible aggregation of LMNPs was observed in the optical microscope prior to placement of the magnet (**Figure 2**a). The magnetic field forced generation of magnetic chains and their translocation in the non-uniform field toward the glass substrate. In 15 s, short chains (l ~ 1–2 µm) were observed in the optical microscope. These chains grew to longer 12–15 µm structures in 60 s (Figure 2b). Similar observations where reported elsewhere.[31]

The chains were stabilized after 15 s of exposure to the magnetic field via the locking mechanism by changing pH to pH 4. Then the droplet was 30-fold diluted with a pH = 4 aqueous solution to prevent interactions between the chains. The sample was dried in the presence of magnetic field when they held their orientation along the field. An AFM visualization was used to monitor the chain formation (as described elsewhere.[32] The AFM image of the chains and a cross-sectional profile along the longest axis of chain 1 is shown in **Figure 3**a and b, respectively. The chains were formed by interconnected single LMNPs. Some chains are formed by merging of two or more chains. The chain were about 2 µm long in average.

After 60 s exposure of the droplet to the magnetic field, the chains agglomerated into bigger bundles. The average length of chains increased from about 2 µm after 15 s to about 15 µm after 60 s (Figure 3c,d). In the non-uniform magnetic field, the chains translocate to the surface of the substrate and form a magnetic coating where the chains become tethered to the

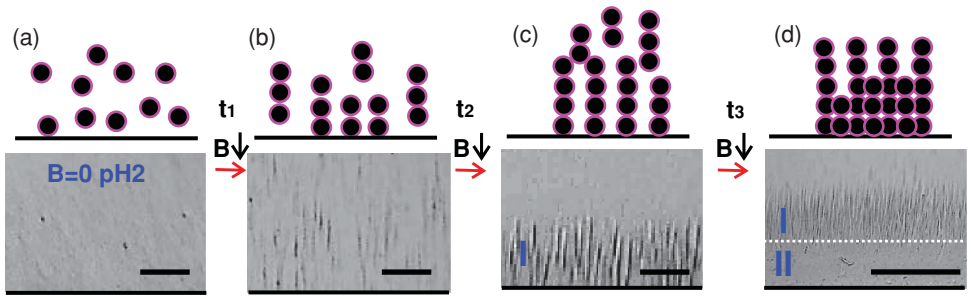

Figure 2. Snapshots and schematics for the formation of an anisotropic coating using 0.8 g/L aqueous solution of LMNPs in a non-uniform magnetic field, the field direction is shown by the arrows; scale bars are 100 μm for all images: a) No aggregation was observed prior to application of the magnetic field at pH 2; b) When the magnet was placed, short chains appeared throughout the area of the droplet; c) chains move to the glass surface and formed a forest-like structure; d) The coating grows via two propagating fronts: I propagating by the head-to-tail attachment of the chains arriving from the bulk solution to the forest of magnetic chain, and II propagating of the densely packed film by translocation of magnetic chains into the forest between the tethered chains.

substrate and aligned into a forest-like structure (Figure 2c). The development of the coating in time is shown in Figure 2 and the dynamic process is demonstrated in a movie file of SI.

It is clearly seen in the movie that until some critical time $t_{cr} \approx 60$ s (about 7–8 s for Video 1), the arriving chains would attach to the glass slide surface and to the tethered chains into the tail-to-head configuration; after that critical time they translocate in between the tethered chains increasing the density of the forest-like structure. In the course of the coating formation, we observe two propagating fronts that demark two interfaces

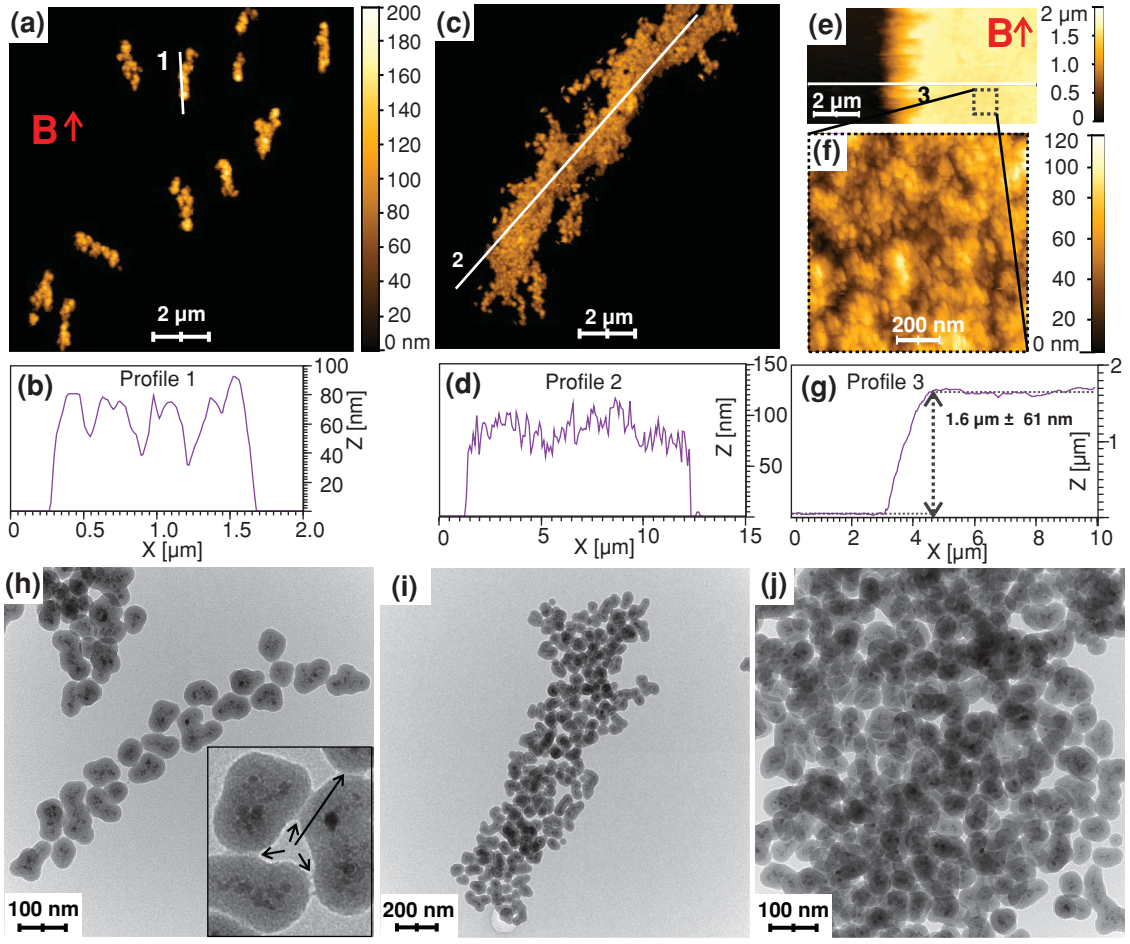

Figure 3. AFM images of magnetic chains stabilized after 15 s in the magnetic field (0.8 g/L solution of LMNPs): a) Topographical images of the chains adsorbed on the Si-wafer; b) a long axis profile of chain 1 (labeled in the a-panel); c) chain 2 after 60 s growth in the magnetic field and d) its profile; e) surface topography of the densely packed forest of the chains in the z–y plane and; f) profile along the line 3 (labeled in the e-panel) showing that the tethered chains are densely packed and form a solid film; h–j) TEM images of magnetic chains, arrows show the polymer layers connecting particles.

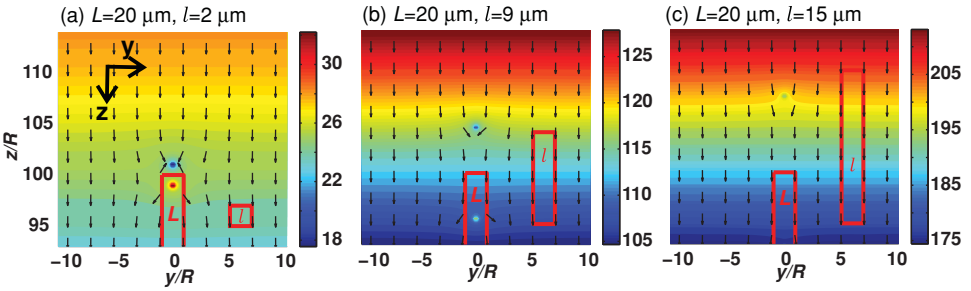

Figure 4. Potential energy U, and force distribution for coming chains (l) at a constant length of the tethered chains (L); black arrows indicate the direction of the force; color contrast shows potential energy variation marked with color bars: (a) L = 20 μm, l = 2 μm, (b) L = 20 μm, l = 9 μm, (c) L = 20 μm, l = 15 μm.

(Figure 2d): (a) the front at the interface of the bulk solution and the forest of chains when the front is propagating by the tail-to-head growth mechanism and (b) the front at the interface of the magnetic forest-like structure and the "saturated" densely packed film of the magnetic chains when the front is formed by densely packed chains. The coating develops until supply of the magnetic chains from bulk solution lasts.

The mechanism of coating formation can be rationalized by considering a combination of several phenomena: formation of magnetic chains, translocation of LMNPs and the magnetic chains to the substrate surface and increasing the local concentration of the particulates (particles and chains) at the liquid-solid interface. The effect of particle concentration on the chain formation was analyzed by Furst and Gast[33] when several concentration regimes where discriminated in the phase diagram to demonstrate alignment of chains, their aggregation, branching and formation of rigid structures with increase in volume fraction of particles and strength of magnetic field. In our experiments, the mechanism of the film formation appears to be a more complex dynamic process in a non-uniform magnetic field due to an intricate competition between the dipole-dipole forces F_{dd} acting between the incoming and tethered chains and the forces caused by the field gradient F_g. When $F_{dd} > F_g$ the incoming chain is expected to land right at the head of the tethered chain increasing its length. When $F_{dd} < F_g$ the chain is expected to pass by the tethered chains moving towards the substrate surface. After landing at the substrate the chains become tethered by the field gradient. Since the incoming chains grow on their way to the substrate, the scenario of chain landing significantly depends on the initial concentration of the LMNPs and the particle magnetization. Time t_{cr} can be therefore associated with the change of a sign of the inequality $F_{dd} > F_g$: in time t_{cr} the chains were grown above the critical length when the force due to the magnetic field gradient overcame the dipole-dipole force, $F_{dd} < F_g$, and the chains translocated inside the chain forest.

2.2. Theoretical Model of the Coating Formation

A theoretical model developed in this work explains the transition from the regime of growing tethered chains to the regime of chains translocation into the forest of tethered chains by filling the gaps between chains. It is assumed that a chain of length L has been already tethered to the surface of the glass slide and a chain of length l is arriving to the substrate in the z-direction (**Figure 4**a–c). In our experiments, the z-component of the magnetic field B_z was much greater than the y-component B_y. As a result, the long axis of chain was pointing in the z-direction. For simplicity, we assumed the field gradient $\alpha = \partial B_z/\partial z$ to be a constant in the spot of observation. Using a Hall teslameter and COMSOL solver we obtained the following filed components in this spot B_z = 100 mT, B_y = 0.7 mT and α = 25 T/m. We introduce a new 2D system of coordinates where the position of the arriving chain is characterized by the coordinates of its center of mass taking the center of mass of the tethered chain at the origin of coordinates (0,0). We model chains by circular cylinders with magnetization M_s, and radius R. The effective magnetic charge at each south and north poles is therefore equal to $\pi R^2 M_s$. The magnetostatic energy between two chains is associated with the energy of their magnetic poles.[34] Adding the magnetostatic energy associated with the external magnetic field, the total energy is written as:

$$\frac{U}{\frac{\mu_0}{4}M_s^2\pi R^3} = \left(\frac{1}{\sqrt{(y/R)^2+(z/R-l/2R+L/2R)^2}} + \frac{1}{\sqrt{(y/R)^2+(z/R+l/2R-L/2R)^2}} - \frac{1}{\sqrt{(y/R)^2+(z/R-l/2R-L/2R)^2}} - \frac{1}{\sqrt{(y/R)^2+(z/R+l/2R+L/2R)^2}} \right) + \frac{4\alpha l}{\mu_0 M_s}\frac{z}{R} \quad (1)$$

where μ_0 is the vacuum permeability. The total force acting on the moving chain of length l is calculated as:

$$F_y = -\frac{\partial U}{\partial(y/R)}, F_z = -\frac{\partial U}{\partial(z/R)} \quad (2)$$

Since the term $4\alpha l/\mu_0 M_s$ is proportional to l, increasing the length of arriving chain will significantly amplify the effect of the field gradient on chain landing.

The magnetostatic energy and force distributions are shown in Figures 4a–c. Following parameters we used for the calculations: magnetization of Fe_3O_4 $M_s = 2 \times 10^3$ A/m, R = 1 μm, L = 200 μm as the most relevant to the experimental conditions. The length of the coming chain was varied from 2 μm to 15 μm to follow the experimental observations. Black arrows indicate

the direction of the force acting on the center of mass of the coming chain. The color represents the dimensionless energy normalized by $\mu_0 M_s^2 \pi R^3/4$. The force distribution in Figure 4 is in excellent agreement with the experimental observations: when the length of the arriving chain is less than 9 μm, the chain lands atop the tethered chains. When the length of an arriving chain is greater than 9 μm, the chain passes by the tethered chains and lands at the surface of the substrate. As soon as the substrate surface is covered by densely arranged chains, the further frontal propagation of the coating develops by landing of arriving chains on the top of the densely tethered chains so that two layers (lower dense and upper less dense) grow in a steady-state regime as long as the particle supply lasts.

2.3. Formation of the Anisotropic Structure

The discovered mechanism of the coating formation could be used to regulate thickness and density of LMNPs chains while the locking mechanism is used to stabilize the anisotropic structure of the coating at any stage of the coating formation. The latter we demonstrate with the experiments discussed below.

Formation of the forest-like structure on the surface of the glass slide was monitored in an aqueous suspension of LMNPs at pH 2 (**Figure 5**). The generated coating was then stabilized by adding a small portion of a pH 9 aqueous solution to adjust pH > 4 in the cell. The magnet was removed and the forest-like structure remained stable due to the locking effect (Figure 5c). At the same time, the chains that arrived to substrate surface were bound to the glass substrate due to electrostatic and strong van der Waals interactions between P2VP blocks and the negatively charged glass surface (Figure 1e). It is important, that the terminal particles in the arrived magnetic chains are irreversibly adhered to the glass substrate. Thus, attachment and detachment of the chains are realized via the locking mechanism acting between the particles adhered to the glass substrate and the rest of the chain. No noticeable damage of the structure was detected in 2 h after the field removal in contrast to reference experiments with non-locking particles. In the reference experiments, the forest-like structure was disintegrated immediately upon removal of the magnet, while the densely packed coating disintegrated slowly.

A similar experiment was conducted with a droplet located in the area where the magnetic field was directed at the 30° angle with the surface of the glass slide (Figure 5d). First, the forest of chains was formed perpendicular to the surface at pH 2 as described above. Second, the glass slide was moved to the spot where the magnetic field makes a 30° angle with the surface and chains were locked in this state by changing pH to pH > 4. Figure 5e shows the magnetic chains locked at 30 degrees with the base of glass slide after removing the magnet. The locked structures cannot be changed by changing in the field directions. Movement of the magnet to different positions resulted in no changes in the chain alignment. Then, the magnet was removed and pH in the droplet was decreased to pH 2. The structure was erased by thermal fluctuations (Figure 5f). The magnet was placed at the glass slide to recover the structure and the slide was moved to the spot where the magnetic field makes a −30° angle with the surface and chains were locked in this state by changing pH to pH 4 (Figure 2g). Video2 (see SI) demonstrates the above described experiment in dynamics.

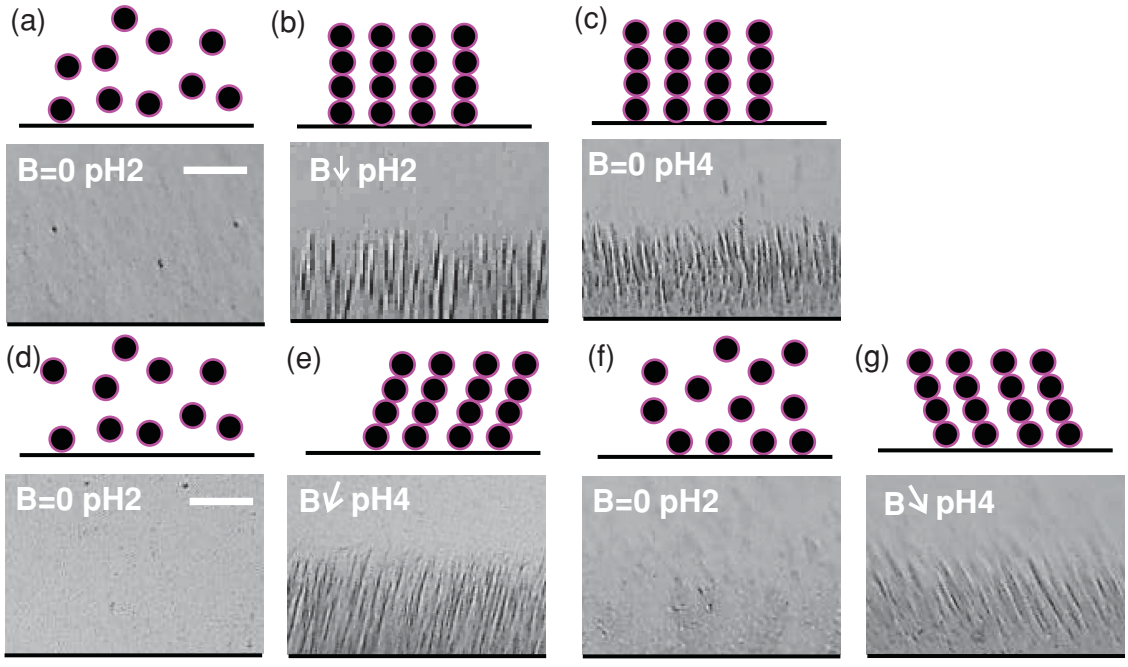

Figure 5. Stabilization, disintegration, control of anisotropy and reconfiguration of the coatings made of LMNPs; the field direction is shown by the arrows: (a,d) stable dispersion of LMNPs at pH 2 demonstrates no aggregation; (b) formation of an anisotropic forest-like structure of the coating in the magnetic field; (c) locking the structure by adjusting pH > 4; (e) formation of the forest-like structure at the 30° angle with the surface of the glass slide at pH 2 and locking at pH > 4; (f) erasing of the structure at pH 2; (g) formation of the forest-like structure at the −30° angle with the surface of the glass slide at pH 2 and locking at pH > 4.

The optical images of the generated coatings in Figure 5 demosntrate anisotropic optical properties of the material. For quantitative characterization of swichable optical anisotropy of the arbitrary array of magnetic chains we conducted a model experiment using Faraday setup as described in SI (Figures S2, S3; Table S1). In this experiment, we estimated the changes in polaraized monochromatic light as function of the magnetic chains orientation. In magnetic field, the polarization of light should depend on the chain orientation. When the chains were perpendicular to the ***E***-vector, the polarization increased to 0.254 degrees comparing to the isotropic case. On the other hand, when the chains were parallel to the *E*-vector, the polarization decreased to 0.056 degrees comparing to the isotropic case. These results confirm that the allignment if the generated magnetic chains provides switchabe optical anisotropy. The anisotropic properties of the material depend on the dimensions and optical properties of the locking particles, concentrationj of chains and thickness of the coating. Analysis of the anistropic properties of the materails is the subject of ongoing research in our labs.

3. Conclusions

We demonstrated a method of magnetic field directed assembly of magnetic nanoparticles to generate thin anisotropic coatings when the film morphology can be controlled by magnetic field strength, field gradient and particle concentration. A combination with the locking mechanism provides new opportunities for the fabrication of reconfigurable and erasable materials when changes in magnetic field directions and pH of aqueous solution can be used to generate structures, stabilize them, destabilize, reconfigure and stabilize again. It is obvious, that various external stimuli (temperature, light, biological activity, mechanical forces, chemical reactions, etc.) can be applied in a similar scenario for locking magnetic chains and stabilizing the anisotropic coatings.

Supporting Information

Supporting Information is available from the Wiley Online Library or from the author.

Acknowledgements

The research was supported by the National Science Foundation, Grants CBET-0756461, CBET-0756457, and DMR- 1426193, and the Air Force Office of Scientific Research, Grant FA9550–12–1–0459. We would like to thank Chris Plunkett for his help with TEM imaging of nanoparticles.

Received: September 29, 2013
Revised: March 13, 2014
Published online: April 22, 2014

[1] a) M. Grzelczak, J. Vermant, E. M. Furst, L. M. Liz-Marzan, *ACS Nano* **2010**, *4*, 3591–3605; b) Z. H. Nie, A. Petukhova, E. Kumacheva, *Nat. Nanotechnol.* **2010**, *5*, 15–25; c) R. M. Erb, R. Libanori, N. Rothfuchs, A. R. Studart, *Science* **2012**, *335*, 199–204.

[2] a) R. E. Rosensweig, *Ferrohydrodynamics*, Cambrige University Press, Cambrige, **1985**; b) E. Blums, A. Cebers, M. M. Maiorov, *Magnetic Fluids*, Walter de Gruyter, New York **1997**.

[3] a) L. V. Nikitin, L. S. Mironova, K. G. Kornev, G. V. Stepanov, *Polym. Sci. Ser. A* **2004**, *46*, 301–309; b) G. Filipcsei, I. Csetneki, A. Szilagyi, M. Zrinyi, *Adv. Polym. Sci.* **2007**, *206*, 137–189; c) M. Zhu, G. Diao, *Nanoscale* **2011**, *3*, 2748–2767; d) K. Itoh, S. Ishida, M. Hamada, S. Ogawa, *J. Appl. Phys.* **1979**, *50*, 2396–2398; e) T.-W. Chou, *Microstructural Design of Fiber Composites*, Cambridge University Press, Cambridge, UK **1992**; f) S. Ghosh, I. K. Puri, *Soft Matter* **2013**, *9*, 2024–2029.

[4] G. Fosa, R. Badescu, G. C. Calugaru, *Czechoslovak J. Phys.* **2004**, *54*, 989–996.

[5] a) P. Fratzl, *Science* **2012**, *335*, 177–178; b) J. Philip, P. D. Shima, B. Raj, *Appl. Phys. Lett.* **2008**, *92,* 043108; c) P. D. Shima, J. Philip, *J. Phys. Chem. C* **2011**, *115*, 20097–20104; d) G. Filipcsei, I. Csetneki, A. Szilagyi, M. Zrinyi, in *Adv. Polym. Sci.*, Vol. *206*, Springer-Verlag, Berlin **2007**, pp. 137–189.

[6] J. Jestin, F. Cousin, I. Dubois, C. Ménager, R. Schweins, J. Oberdisse, F. Boué, *Adv. Mater.* **2008**, *20,* 2533–2540.

[7] F. Wen-Xiao, H. Zhen-Hui, X. Xue-Qing, S. Hui, *Chinese Phys. Lett.* **2005**, *22*, 2386.

[8] D. Lorenzo, D. Fragouli, G. Bertoni, C. Innocenti, G. C. Anyfantis, P. D. Cozzoli, R. Cingolani, A. Athanassiou, *J. Appl. Phys.* **2012**, *112,* 083927.

[9] M. R. Sommer, R. M. Erb, A. R. Studart, *ACS Appl. Mater. Interfaces* **2012**, *4*, 5086–5091.

[10] F. N. Pirmoradi, J. K. Jackson, H. M. Burt, M. Chiao, *Lab Chip* **2011**, *11*, 3072–3080.

[11] Y. W. Huang, S. T. Hu, S. Y. Yang, H. E. Horng, *Optics Lett.* **2004**, *29*, 1867–1869.

[12] F. Fahrni, M. W. J. Prins, L. J. van Ijzendoorn, *J. Magn. Magn. Mater.* **2009**, *321*, 1843–1850.

[13] N. Hoang, N. Zhang, H. Du, *Smart Mater. Structures* **2009**, *18*, 074009.

[14] M. Jalali, S. Dauterstedt, A. Michaud, R. Wuthrich, *Composites B: Engineering* **2011**, *42*, 1420–1426.

[15] J. S. Leng, W. M. Huang, X. Lan, Y. J. Liu, S. Y. Du, *Appl. Phys. Lett.* **2008**, *92*, 204101.

[16] J. Y. Yuan, Y. Y. Xu, A. H. E. Muller, *Chem. Soc. Rev.* **2011**, *40*, 640–655.

[17] a) A. S. Barnard, H. F. Xu, X. C. Li, N. Pradhan, X. G. Peng, *Nanotechnology* **2006**, *17*, 5707–5714; b) N. Pradhan, H. F. Xu, X. G. Peng, *Nano Lett.* **2006**, *6*, 720–724; c) F. Huang, H. Z. Zhang, J. F. Banfield, *J. Phys. Chem. B* **2003**, *107*, 10470–10475.

[18] M. P. Pileni, *J. Phys. Chem. B* **2001**, *105*, 3358–3371.

[19] A. P. Gast, C. F. Zukoski, *Adv. Colloids Interface Sci* **1989**, *30*, 153–202.

[20] J. D. Carlson, M. R. Jolly, *Mechatronics* **2000**, *10*, 555–569.

[21] A. P. Hynninen, M. Dijkstra, *Phys. Rev. Lett.* **2005**, *94,* 138303.

[22] S. H. Lee, C. M. Liddell, *Small* **2009**, *5*, 1957–1962.

[23] T. Y. Gong, D. T. Wu, D. W. M. Marr, *Langmuir* **2002**, *18*, 10064–10067.

[24] J. J. Benkoski, S. E. Bowles, B. D. Korth, R. L. Jones, J. F. Douglas, A. Karim, J. Pyun, *J. Am. Chem. Soc.* **2007**, *129*, 6291–6297.

[25] Z. H. Zhou, G. J. Liu, D. H. Han, *ACS Nano* **2009**, *3*, 165–172.

[26] E. M. Furst, C. Suzuki, M. Fermigier, A. P. Gast, *Langmuir* **1998**, *14*, 7334–7336.

[27] C. c. Goubault, F. Leal-Calderon, J.-L. Viovy, J. r. Bibette, *Langmuir* **2005**, *21*, 3725–3729.

[28] Y. Xiong, Q. W. Chen, N. Tao, J. Ye, Y. Tang, J. S. Feng, X. Y. Gu, *Nanotechnology* **2007**, *18*, 5.

[29] S. A. Corr, S. J. Byrne, R. Tekoriute, C. J. Meledandri, D. F. Brougham, M. Lynch, C. Kerskens, L. O'Dwyer, Y. K. Gun'ko, *J. Am. Chem. Soc.* **2008**, *130*, 4214.

[30] M. Motornov, S. Z. Malynych, D. S. Pippalla, B. Zdyrko, H. Royter, Y. Roiter, M. Kahabka, A. Tokarev, I. Tokarev, E. Zhulina, K. G. Kornev, I. Luzinov, S. Minko, *Nano Lett.* **2012**, *12*, 3814–3820.

[31] a) S. Z. Malynych, A. Tokarev, S. Hudson, G. Chumanov, J. Ballato, K. G. Kornev, *J. Magn. Magn. Mater.* **2010**, *322*, 1894–1897; b) M. Fermigier, A. P. Gast, *J. Colloid Interface Sci.* **1992**, *154*, 522–539; c) J. H. E. Promislow, A. P. Gast, M. Fermigier, *J. Chem. Phys.* **1995**, *102*, 5492–5498.

[32] J. Jimenez, R. Sheparovych, M. Pita, A. Narvaez Garcia, E. Dominguez, S. Minko, E. Katz, *J. Phys. Chem. C* **2008**, *112*, 7337–7344.

[33] E. M. Furst, A. P. Gast, *Phys. Rev. E* **2000**, *62*, 6916–6925.

[34] K. G. Kornev, D. Halverson, G. Korneva, Y. Gogotsi, G. Friedman, *Appl. Phys. Lett.* **2008**, *9*, 233117.